Z-type Schlieren Setup and its Application to High-Speed Imaging of Gasoline Sprays

Article *in* SAE Technical Papers · August 2011

DOI: 10.4271/2011-01-1981

CITATIONS
9

READS
4,930

4 authors, including:

Sanghoon Kook
UNSW Sydney
185 PUBLICATIONS **3,282** CITATIONS
SEE PROFILE

Srinivas Padala
Indian Institute of Petroleum (IIP)
21 PUBLICATIONS **239** CITATIONS
SEE PROFILE

JSAE 20119146
SAE 2011-01-1981

Z-type Schlieren Setup and its Application to High-Speed Imaging of Gasoline Sprays

Sanghoon Kook, Minh Khoi Le, Srinivas Padala, and Evatt R. Hawkes
University of New South Wales

ABSTRACT

Schlieren and shadowgraph imaging have been used for many years to identify refractive index gradients in various applications. For evaporating fuel sprays, these techniques can differentiate the boundary between spray regions and background ambient gases. Valuable information such as the penetration rate, spreading angle, spray structure, and spray pattern can be obtained using schlieren diagnostics. In this study, we present details of a z-type schlieren system setup and its application to port-fuel-injection gasoline sprays. The schlieren high-speed movies were used to obtain time histories of the spray penetration and spreading angle. Later, these global parameters were compared to specifications provided by the injector manufacturer. Also, diagnostic parameters such as the proportion of light cut-off at the focal point and the orientation of knife-edge (schlieren-stop) used to achieve the cut-off were examined. From the experiment, it was found that a light cut-off of approximately 60% performed the best to image the internal pattern of the gasoline sprays. An interesting finding from the knife-edge orientation study was that a vertically oriented stop increased the contrast of the spray pattern in the vertical direction. Similarly, a horizontal stop showed higher contrast and more turbulent spray structures in the horizontal direction. A combination of a horizontal and a vertical stop therefore unveiled the most of the gasoline spray pattern and structure. The light cut-off proportion and knife-edge orientation, however, did not affect the refractive-index gradient of the spray border and therefore no significant variations in the tip penetration and spreading angle were measured.

INTRODUCTION

Schlieren and shadowgraph imaging are powerful tools to study turbulent multiphase flows. Despite the fact that limited quantitative data can be obtained, schlieren imaging can visualize internal structures of the gas-phase fluid flow, which is invisible without a proper optics setup. Also, it is relatively simple and cheap to build compared to costly planar-laser-based diagnostics. As a result, the schlieren setup has become very popular and is widely available.

Details of the theory and diagnostic considerations of the schlieren technique are readily available in many fine textbooks. For example, presenting a wide range of example images, Settles [1] has already discussed almost all parameters of concern in the schlieren setup. However, the discussions are for simple example cases and lack the details needed to study more complex fuel spray behavior. This study, therefore, aims to bridge the gap between fundamentals of the schlieren setup and application details for fuel spray imaging.

In automotive applications, schlieren imaging has been widely used to study fuel sprays [2-7] or gaseous fuel jets [8-9] in engine environments. Often an optical chamber is used to decouple fuel sprays/jets from turbulent in-cylinder flow [2-4, 8]. Also, schlieren imaging has been attempted in more challenging environments such as optical engines [5-7] or a rapid compression machine [9]. There are three types of schlieren systems that are commonly used in automotive research: (i) lens systems (*e.g.* [2, 3]), (ii) double-pass mirror systems (*e.g.* [7, 8]), and (iii) z-type mirror systems (*e.g.* [4-6, 8, 9]).

Lens systems are generally simple and easy to set up as they follow the “straight” layout as displayed in Fig. 1. For example, evaporating diesel sprays [2] or gasoline/ethanol sprays [3] have been studied using lens systems. Light was generated from either a laser or projection lamp, passed through a pin hole and was then collimated by a magnifying lens. The simplicity of such lens systems offers a great advantage as there is no off-axis aberration, which is the biggest challenge in mirror systems (to be discussed in greater detail later in the paper). Despite this advantage, the lenses in this type of schlieren system are required to be of very high quality, which leads to high cost and high maintenance level. Also, lenses are restricted in size: their diameters cannot be as large as parabolic mirrors, meaning that these systems cannot be used to observe a large region of interest. Due to its straight layout, the lens system is also longer in length (requiring more space for the total arrangement) than mirror-based systems.

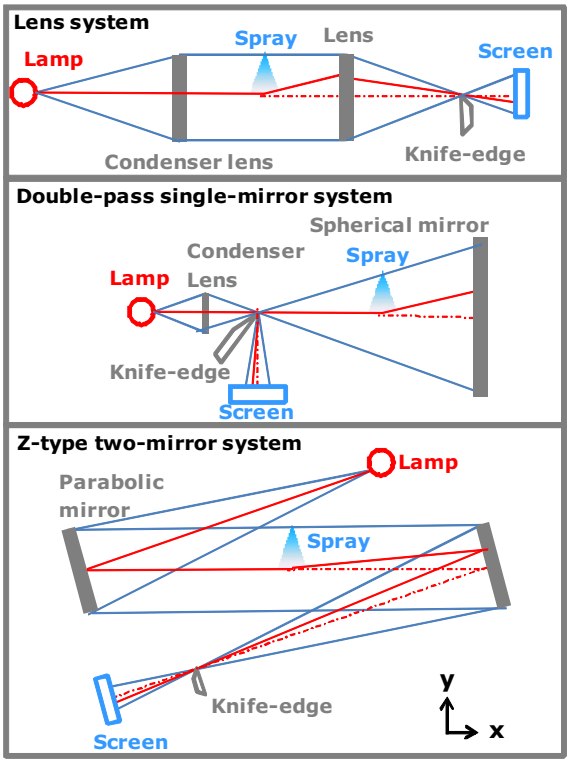

Figure 1: Sketch of optics and light paths for various schlieren setups.

The double-pass mirror system uses only one mirror, missing out on the advantages of collimating light rays. This arrangement is also known as the single-mirror coincident system. As illustrated in Fig. 1, a single spherical field mirror with the light source on axis at the radius of curvature is used. Alternatively, a parabolic mirror with a corrector lens after the light source can be used. The schlieren object is positioned in front of the mirror. The principle is that, as the diverging light beam passes through the schlieren object, it hits the mirror and returns along a coincident path, forming an image. Afterward, a reflecting knife-edge or beam splitter separates the returning rays from the source rays. These returning rays then carry the schlieren image to a camera.

In this system, since the light passes through the schlieren object twice, the deflection of light rays occurs twice resulting in increased sensitivity. This in fact increases the sensitivity as the refraction angle is small and the schlieren object is close to the mirror where light is more uniformly dissipating. If the setup is in perfect coincident on-axis, off-axis aberrations are completely eliminated. However, the double-pass setup requires a rather large, high-quality mirror which drastically increases the cost. Also, the light rays are not propagating parallel to each other and the schlieren object is close to the mirror, which is a disadvantage in some applications. These limitations are well demonstrated in Ref. [7]: in an optical-accessible engine, a double pass schlieren system was used to visualize evaporating diesel sprays. A metal mirror attached on the injector-mount plane was used as the main mirror in their system. The authors found that by modifying illumination angle, image patterns would change. For instance, higher angles filtered out the information about the gas flow structure, which resulted in the spray being presented with a higher contrast in the image. However, there were some limitations such as the need for filtering the reflections on the optical access window surfaces and requirements for a high quality mirror appropriate for high pressure and temperature conditions inside the combustion chamber. Petersen and Ghandhi [8] used a similar system with the inclusion of a large circular mirror with a hole to accommodate the fuel injector tip. They used a parabolic mirror to make light rays coming from the light source shine on this circular mirror. This parabolic mirror was also tilted in a way such that the refracted beam was separated from the original light path. This decreased the difficulty in setup and avoided the use of beam splitter; however, it introduced some off-axis aberration.

The z-type two-mirror system is the most popular schlieren system setup in practice. This is because the system allows a larger test region without needing to increase the size of the mirrors. As shown in Fig. 1, light generated from a light source focuses on a condenser lens and goes through a slit. It is then directed to a parabolic mirror and collimated, resulting in uniform propagation through the test region. The collimated light is incident on another parabolic mirror, which refocuses the light rays. The light passes through a cut-off (an edge or filter) and is refocused onto a screen or an image sensor of a camera. In general, light rays travel in a z-shaped, hence the title.

Due to the parallel light shone through the schlieren image and the space between the two mirrors, this set up is particularly useful for imaging a two-dimensional schlieren object. For example, Pickett *et al.* [4] used this system to visualize reacting diesel jets, providing insight into the time sequence of diesel ignition and combustion. Also, useful tips for the z-type schlieren system were found: including a small 5° angle for low astigmatism and the fact that the shadowgraph technique (no light cut-off) was more than sufficient to detect the edge of the jet, possibly due to high refractive index gradients that existed in the high-density environment. In-cylinder phenomena of gasoline engines have also been studied using the z-type schlieren system [5, 6]. Due to the curvature in the cylinder liner, the setup of schlieren imaging in an optical engine is more challenging. By manipulating the outer shape of the cylinder, however, it was found that light could be collimated through the region inside the engine cylinder. The importance of a well-defined, point-like light source in the z-type system is well demonstrated in Ref. [8] where a f/1.4 condenser lens was employed (allowing a large amount of light to pass through) together with a 1 mm pin hole.

While schlieren diagnostics are well-developed and do not fall into the category of “advanced” diagnostics, there is still room to improve them, particularly for automotive applications. For example, schlieren-stops with a different orientation may improve the schlieren image quality in the case of fuel sprays. Diagnostic

details such as selection of the light source and the technique to create collimated light for the best uniformity can also affect clarity of the fuel spray significantly. Limitations imposed by the space-requirement of the setup are quite common in automotive experiments and must be considered. However, how these numerous setup parameters affect the quality of schlieren signals tends to stay in-house and has not been shared in the open literature.

One of the primary objectives of this study is to present a z-type schlieren imaging system with the ultimate goal of improving the schlieren signal of gasoline sprays. From our survey of the literature [4-6, 8, 9], the z-type schlieren system has been identified as the most common setup in engine applications. It has certain advantages of simplicity and sensitivity that make it attractive in comparison to other setups. Also, to image gasoline sprays, in which geometric and structural information is of particular interest, space is required to accommodate a fueling system, and an optical chamber is required to achieve relevant ambient conditions. Therefore, we concluded that a z-type system is the most suitable to study gasoline sprays.

High-speed schlieren imaging [2-9] also offers room for improvement. The continuing advancement in high-speed camera technologies increases the potential to understand the transient behavior of sprays. Compared to film-based high-speed cameras or earlier version digital high-speed cameras, new cameras offer superior image quality, high framing rates, and very fast data processing. This may enable us to understand transient nature of fuel sprays, which was previously inaccessible due to the long gating time of older cameras.

In this study, the details of the z-type schlieren setup are discussed: including mirrors, a light source, a camera, and schlieren stop. We have applied the developed technique to gasoline spray imaging. Specifically, a high-speed imaging at 11,527 frames per second was performed to uncover the transient behavior of gasoline sprays. Details of spray image processing are also discussed. Finally, we have examined diagnostic parameters such as the proportion of the light cut-off at the focal point and using a combination of a horizontal and a vertical cut-off to optimize the schlieren signal.

BRIEF SUMMARY OF SCHLIEREN AND SHADOWGRAPH THEORY

A schlieren signal is a result of refractive-index gradient. In fuel sprays, temperature or density variations at the boundary between evaporating fuel and ambient gases lead to disturbances that refract light, and these can be detected with the proper setup. An example of schlieren imaging for evaporating gasoline spray (*i.e.* schlieren projected on a screen) is shown in the left side of Fig. 2. Defining the x coordinate as an axis of the light rays, the schlieren image is shown on a y-z plane. It is clear that the evaporating gasoline spray remains visible above the background with a more uniform structure.

In the geometric theory of refraction [1], the curvature of a refracted light ray is a function of the refractive-index gradient through which it passes *i.e.*

$$\frac{\partial^2 y}{\partial x^2} = \frac{1}{n}\frac{\partial n}{\partial y} \quad , \tag{1}$$

where n is the refractive index. To apply this formula to the gasoline sprays, the simple case of a positive vertical refractive-index gradient ($\partial n/\partial y$ >0) at the spray border (annotated as "A" in Fig. 2) is assumed, while no gradient is assumed to exist in the *x* or *z* directions.

The sketch in the right side of Fig. 2 illustrates that n_2 is higher than n_1 and therefore the light ray is turned to a counter-clockwise angle $\Delta\varepsilon$ following Huygens' principle. The light is collimated prior to the spray region and is hence initially normal to *y*-axis upon passing through x_1. As the light ray propagates through the spray region from x_1 to x_2 for a differential time Δt, it is refracted through the differential angle $\Delta\varepsilon$. Using the light speed c and the speed of light in a vacuum c_0, this angle can be expressed as:

$$\Delta\varepsilon = \frac{(c_0/n_1 - c_0/n_2)}{\Delta y}\Delta t \tag{2}$$

Substituting $\Delta t = \Delta x \cdot n(y)/c_0$, adopting $n(y) \approx n_1 \approx n_2$ as $\Delta y \to 0$, and finally letting all the finite differences approach zero, it is obtained that:

$$\frac{d\varepsilon}{dx} = \frac{1}{n}\frac{dn}{dy} \tag{3}$$

From Eq. 3, assuming ε is very small and hence $\varepsilon = dy/dx$, the curvature of the refracted ray can be expressed as:

$$\frac{d^2 y}{dx^2} = \frac{1}{n}\frac{dn}{dy} \tag{4}$$

Note that by writing the total derivatives as partials to account for other refractive-index gradients, Eq. 1 is obtained.

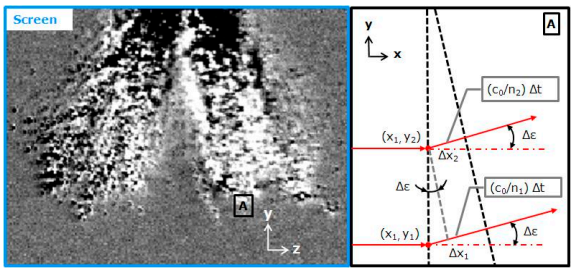

Figure 2: An example of schlieren image (left) and simplified sketch of refracted beam path near the spray tip (right).

Furthermore, by integrating Eq. 3 for the surrounding medium of refractive index n_0 and a two-dimensional schlieren object of extent L along the optical axis, the angular ray deflection ε in the y- and z- direction can be expressed as:

$$\varepsilon_y = \frac{L}{n_0}\frac{\partial n}{\partial y}, \text{ and } \varepsilon_z = \frac{L}{n_0}\frac{\partial n}{\partial z} \quad (5)$$

Above equations provide a theoretical basis for differentiating schlieren and shadowgraph imaging techniques. In shadowgraph imaging, a disturbance, *i.e.* a deflection angle gradient ($\partial\varepsilon_y/\partial y$ or $\partial\varepsilon_z/\partial z$) is observed in the form of ray displacement. Using Eq. 5, this means that the second derivative of the refractive index ($\partial^2 n/\partial y^2$ or $\partial^2 n/\partial z^2$) is visualized in the shadowgraph imaging. Equation 5 also shows that the shadowgraph technique cannot image fluid flows if the presented refractive-index gradient is uniform (*i.e.* $\partial n/\partial y$ and $\partial n/\partial z$ is constant). This uniform gradient shifts the entire light rays undisturbed (or ε_y and ε_z is constant in Eq. 5) and hence no shadowgraph may be imaged. By contrast, the schlieren technique can visualize flows with a uniform refractive-index gradient. By placing a knife-edge at the focal point (see Fig. 1), some of the deflected rays are blocked (or "disturbed") and therefore a phase difference is created. This phase difference then can be projected on the screen or can be detected by the camera sensor. Therefore, the schlieren signal is proportional to the first derivative of the refractive index ($\partial n/\partial y$ or $\partial n/\partial z$). This results in higher contrast and sharper edges for schlieren images than those for shadowgraph images. On the other hand, the use of a schlieren stop makes the images darker. This trade-off must be considered to decide whether to place the stop (schlieren) or not (shadowgraph).

SCHLEREN OBJECT

OPTICAL CHAMBER AND GASOLINE SPRAYS

Measurements were obtained in an optically accessible, constant-volume spray chamber in which tailored ambient temperature and pressure conditions corresponding to typical gasoline engine intake systems can be provided. Schematics of the chamber and schlieren measurement setups are shown in Fig. 3. Sight-glass windows are located in three sides of the chamber to allow line-of-sight and orthogonal imaging of the injected fuel spray. The ambient pressure and temperature conditions are achieved in the chamber using an air compressor and heater. For example, the chamber is capable of simulating intake boosting of up to 200 kPa. Since experiments in this study were performed at standard laboratory ambient conditions, however, there was no need of running a compressor and heater.

A port-fuel-injection (PFI) injector was used to study gasoline sprays. While PFI injectors have been available for more than two decades and more advanced direct-injection injectors are rapidly penetrating the market, PFI sprays are of particular interest because hardware and control systems still have economic benefits and superior reliability. Considering these, we selected a conventional PFI injector to demonstrate our schlieren imaging system.

A Bosch PFI injector (MPI Model EV-6) equipped with six orifices ("director plate" multi-orifice) was used for this study. According to the injector manufacturer's specifications, the spreading angle ($\alpha_{80\%}$) was 70°: by Bosch's definition, 80% mass of sprays was within $\alpha_{80\%}$. The fueling rate measured, at 300 kPa of orifice pressure drop, was 382 cm^3/min. Physical properties of the gasoline used in this study are also given in Table 1.

SCHLEREN OPTICS AND SETUP

OFF-AXIS ABERRATIONS AND MIRRORS

The z-type schlieren system involves some challenges, mostly due to the fact that light goes off axis in its path. Namely, off-axis aberrations are created when the captured light is not on the axis from which the light was generated. Two most common off-axis aberrations effects are "coma" and astigmatism.

Comatic aberration (or coma in short) occurs when light is reflected from the mirror on an angle. The image of a point is focused at sequentially differing heights, producing a series of asymmetrical spot shapes of increasing size that result in a comet-like structure [10]. However, the coma can be corrected by using a combination of lenses that are positioned symmetrically around a central stop. This is particularly useful in z-type schlieren systems, where combinations of two identical mirrors are used and hence the tilt angles of the mirrors could be arranged to be symmetrical.

Astigmatism is the failure of focusing a point to a point, and the image is therefore not properly focused. Rays that propagate in two perpendicular planes have different foci, which means that, as light travels in two waves, horizontal and vertical, horizontal lines will be focused at a different place compared to vertical lines. Astigmatism is shown to be proportional to the square power of the off-axis angle [11] hence it can be reduced by reducing the size of the off-axis angle. The longer focal length obtainable with parabolic mirrors can also help reduce astigmatism. In the present setup, the angle created by the illuminator path (between light source and first mirror) and the collimated path (between the two mirrors) was twice the off-axis angle, so any reduction in this angle would only count as half the reduction in the off-axis angle.

We chose quality mirrors with high surface accuracy of λ/8 and enhanced aluminium coating. To minimise the coma, the focal length and f-numbers of the mirrors were maximised. At the same time, limitations of the test space had to be considered. As a result, a

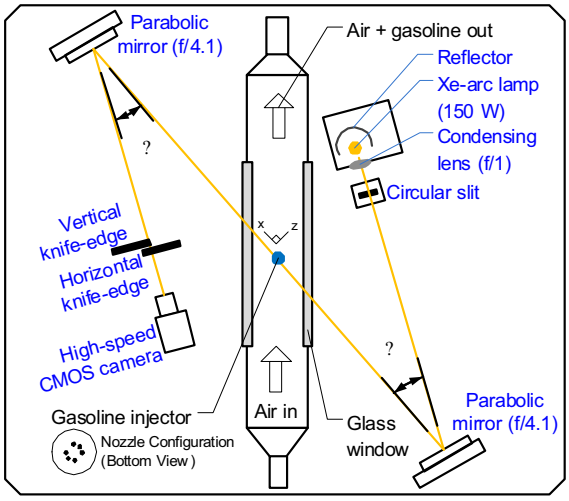

Figure 3: Schematic of schlieren optics setup and light path.

Table 1: Operating conditions

Ambient air	
Pressure [kPa, gauge]	0
Temperature [K]	295
Fuel injector	
Injector type	Bosch MPI EV-6
Number of holes	6
Injection pressure [kPa]	250
Spreading angle [°, $\alpha_{80\%}$]	70
Gasoline properties	
Vapor pressure [kPa, absolute]	45~90
Density [kg/m^3]	720 (15 °C)
Viscosity [Pa-s]	0.00042
Surface tension [N/m]	0.0189
Flash point [°C]	-43
Heat of vaporization [kJ/kg]	310
Boiling point [°C]	30~200

mirror with the aperture of f/4.1 with a focal length of 444.5 mm was chosen.

For the positioning, there should be at least a distance of twice the focal length between the two mirrors to provide space for the test area; therefore, a minimum distance of 890 mm was required. Considering the size of the spray chamber (260 mm in the optical path), the minimum distance is increased to 1150 mm. In the actual set up, the distance between the mirrors was 1450 mm.

LIGHT SOURCE

As the positions of the mirrors were now fixed, the illuminator path had to be moved. This required the positioning of the light source to be as close to the collimating path as possible as shown in Fig. 3. As the collimating path crossed over the spray chamber, it acted as a constraint in the positioning of the light source in this experiment. Hence, the light source should be as close as possible to the chamber. Obviously, the distance between the slit source and first mirror is to be at least the focal length of the mirrors. In the present setup, the distance on the illuminator path was 450mm, slightly longer than a mirror focal length of 444.5 mm.

Others have used continuous-wave lasers [5-6, 9] as a light source because of a constant supply of high power. However, a modern Xe-Arc lamp performs well for the same purpose [4, 8]. We used a 150-W (electrical power) mercury-xenon arc lamp as a white light source in this experiment. To collect radiation off the back to the lamp and direct it through the optical system, a reflector was also placed behind the lamp. For the focusing, a f/1 condensing lens was used and the light was spatially-filtered through a 1-mm aperture.

HIGH-SPEED CAMERA

Using the second parabolic mirror, which was nominally identical to the first mirror, the collimated beam was re-focused into a high-speed camera (VisionResearch Phantom v7.3). Containing a CMOS sensor with size of 17.6 mm by 13.2 mm (22 µm pixel size) and quantum efficiency of 31% at 530 nm, this camera is capable of taking up to 500,000 frames per second. However, these frame rates were only available at very low resolutions of 32-by-32 pixels, which was not enough to capture the gasoline sprays of this study. Therefore, we selected 512-by-512 pixels at the maximum framing rate of 11,527 frames per second.

The lens used for this camera was a 50-mm Nikon Nikkor lens. With a wide aperture of f/1.4, the lens allowed a maximum amount of light reaching the sensor of the camera, which was essential for the schlieren imaging. A focal length of 50 mm provided a suitable field of view, with horizontal field of view (FOV) angle of 39.6^0, vertical FOV angle of 27^0 and diagonal FOV angle of 46.8^0. The exposure time was fixed at 2 µs, which was the minimum value of the camera, to avoid saturation of the bright background as well as blurring of the fast-moving sprays. For the shadowgraph imaging setup with no schlieren stop, however, the saturation was unavoidable due to a high power Xe-Arc lamp and therefore a neutral density filter with an optical density of 0.5 was used.

SCHLIEREN STOP (KNIFE-EDGE)

Intuitively, the successful and correct positioning of the schlieren stop will uniformly darken the image captured. In other words, if the schlieren stop was incorrectly positioned, it would be easily noticeable because of the partial darkening of the image and the apparent difference in brightness. Figure 4 shows some examples. The image at the top-left shows a case with no knife-edge. Below this image, a vertical knife-edge was introduced from the left side of the camera and was incrementally moved along the light path axis until the knife-edge was at the vertical focus point. From there, it could be incremented toward the right side of the camera, perpendicularly to the analyser axis. The horizontal knife-edge was also put

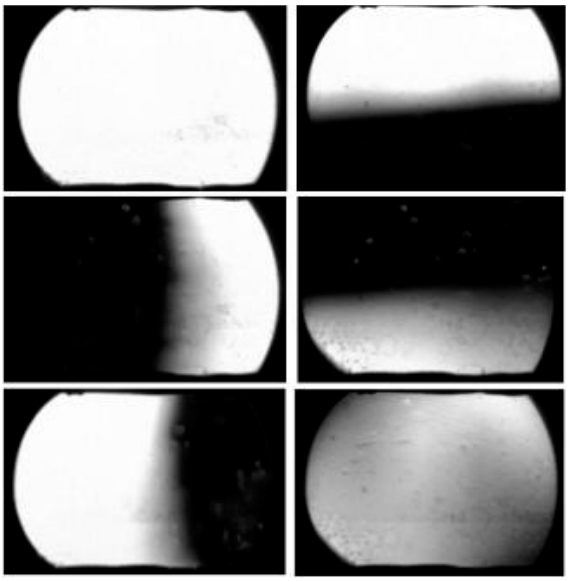

Figure 4: Schlieren images of the chamber prior to fuel injection (*i.e.* background image) during the knife-edge setup.

through the same 'tuning' process. This cut-off was introduced from below the light path. It was also moved along the axis until the correct position was found. From that position, the amount of light cut-off was controlled by the knife-edge movement in the plane perpendicular to the light path axis. The result with a correct knife-edge position is shown at the bottom-right.

SCHLIEREN IMAGE PROCESSING

BACKGROUND CORRECTION AND SPRAY BOUNDARY DETECTION

An example of schlieren images with no schlieren stop (*i.e.* shadowgraph) is shown in Fig. 5. In the first column of the figure, still images obtained from a movie of gasoline sprays are shown. The time after the start of injection (aSOI) is stamped at the each image top-left.

The image at 1 ms aSOI shows that soon after the injection starts, evaporating sprays penetrate downstream and are clearly visible above the near-uniform background. The spray droplets continue to travel across the chamber while maintaining the overall structure during the injection period as demonstrated in the image at 3 ms aSOI. At 5 ms aSOI, when the injection stopped, small droplets are seen in the near-nozzle region.

In Fig. 5, white solid lines are overlaid on the spray images to annotate the spreading angle ($\alpha_{80\%}$ = 70°). By Bosch's definition, 80% of fuel mass is within $\alpha_{80\%}$ when the injector is tested using a mechanical patternator [12]. Since schlieren images are light-of-sight integrated, a direct comparison between $\alpha_{80\%}$ and measured spreading angle from the images is not possible. However, a visual inspection indicates that majority of fuel droplets present within $\alpha_{80\%}$ and the spreading angles show a reasonable match. Later in the following section, we will propose a method to determine the spreading angle, which fits $\alpha_{80\%}$ well regardless of the schlieren sensitivity.

As discussed earlier in the section on Schlieren and Shadowgraph Theory, the spray images are a result of the refractive-index gradient created by both liquid- and vapor-phase fuel. Due to this principle, the liquid spray with stronger density gradients (and hence refractive-index gradient) is clearer than the vapor fuels in the schlieren images. For example, vapor fuels near the spray border are transparent and hard to identify. To address this issue, a background correction was conducted. The idea was that the transparent vapor regions would become much clearer by subtracting the background image.

The second column of Fig. 5 shows a result of the background-corrected images (I_{cA}) where the raw image (I_n) was subtracted by the relatively stable background obtained prior to the fuel injection (I_0) – method A. An offset is also added so that the images are shown with more contrast to highlight features of the spray. This is why the spray appears darker, for example. The background correction appears to work well as the ambient now appears uniform, though not perfectly so. The correction scheme capitalizes on one of the advantages of high-speed imaging in that the background immediately before injection is recorded. Background images acquired at a different time, or time-averaged images, would not be sufficient.

With the background correction, more interesting characteristics of the spray penetration are now visible. Indeed, I_{cA} unveils that vapor regions are larger than I_n particularly near nozzle and spray boundaries. For the background-corrected images, a threshold-based boundary-detection was also implemented. The "gray-thresh" function used in this study is Otsu's method [13], which is one of the built-in models in the Matlab software. This method chooses the threshold to minimize the intra-class variance of the black and white pixels and hence is usually a more reasonable choice than an arbitrary choice of the threshold value. Indeed, as is demonstrated in the third column of Fig. 5, boundaries of the spray droplets are successfully obtained using Otsu's method for both liquid- and vapor-phase fuel regions. To illustrate, we also overlaid the detected boundaries on the original image as shown in the last column of Fig. 5.

Although I_{cA} was effective as demonstrated in Fig. 5, the structure in the background of the shadowgraph actually does change slightly during the course of injection. Therefore, we also attempted another background correction method that used the background from a preceding image for the correction similar to Refs. [4, 14] – method B. By subtracting successive images, variations in the background can be eliminated. For example, the imaging interval was 87 μs in which the background did not change significantly while the droplets travelled about 10

pixels (=1.85 mm). Figure 6 shows this result (I_{cB}), which is the intensity of the current image (I_n) minus the intensity of the previously acquired image (I_{n-1}). For the purposes of presentation, a grayscale offset was also added. In the images, turbulent spray patterns are well captured (the second column) and the boundary detection was more effective (the third column). Indeed, new boundaries overlaid on the original shadowgraph images (the last column) show that the internal spray pattern is well captured including small-scale structures, which is not possible in the simple correction using the intensity of the background prior to injection (I_{cA}).

How these two different correction methods apply to more sensitive schlieren images is demonstrated in

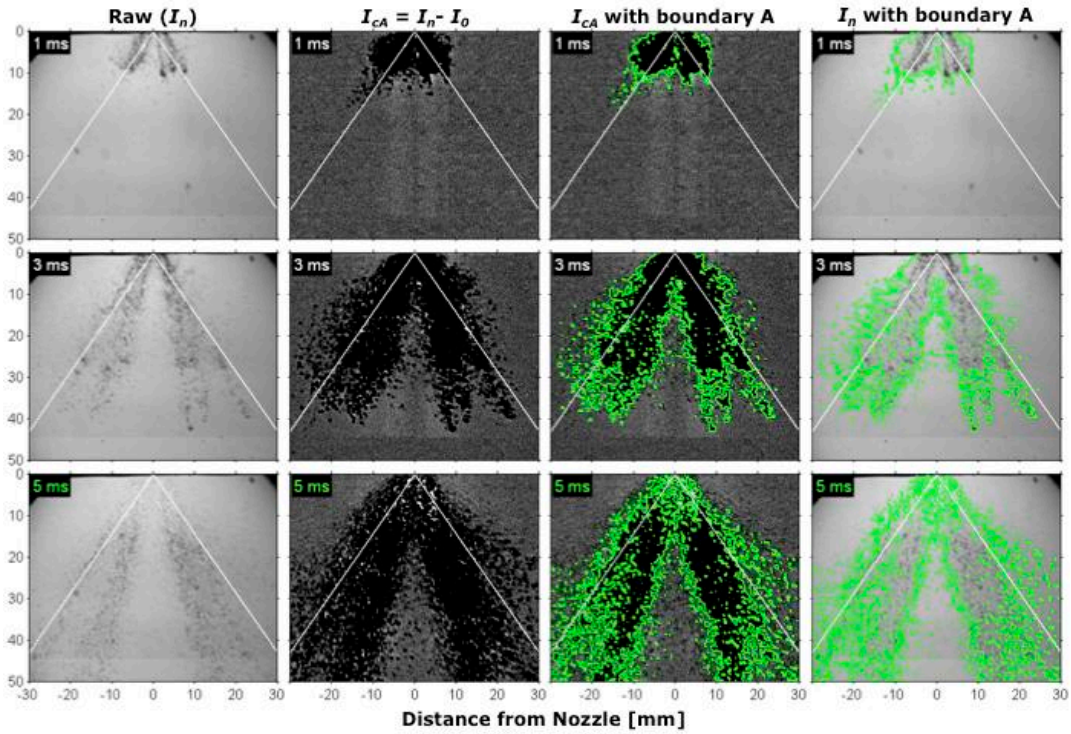

Figure 5: Original shadowgraph images and corrected images using background-correction method A. Solid white lines are drawn using a spreading angle provided by the injector manufacturer (80% mass angle). Shown at the image top-left is time after the start of injection.

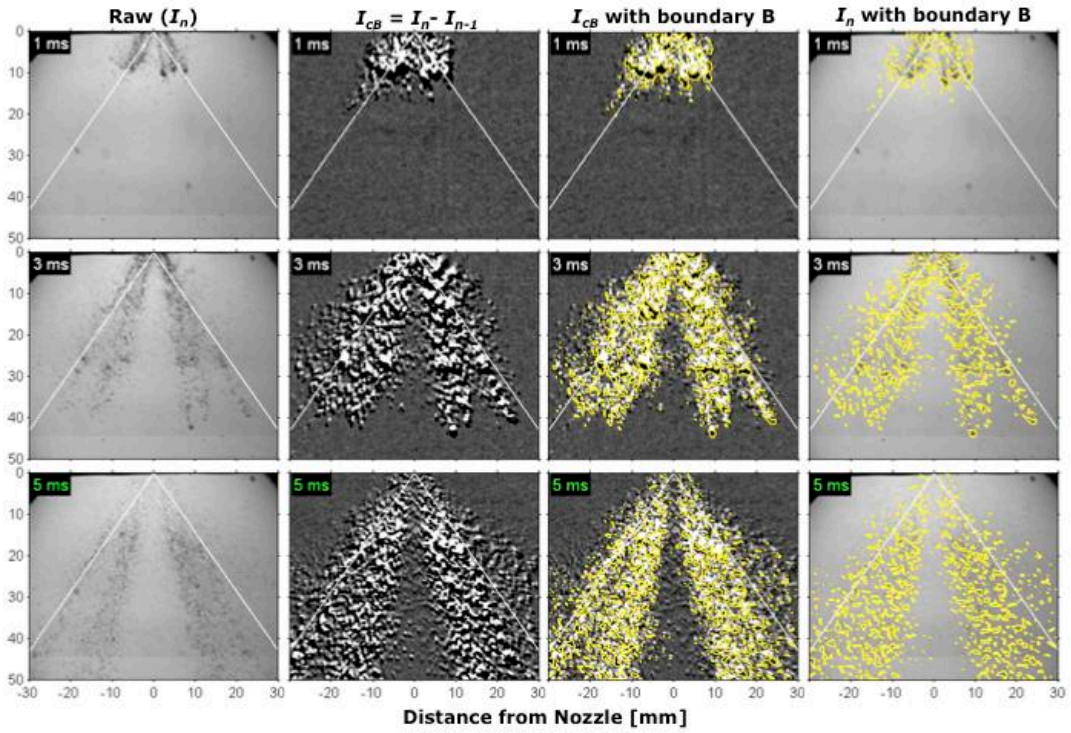

Figure 6: Original shadowgraph images and corrected images using background-correction method B.

Fig. 7. Using both I_{cA} and I_{cB} methods, the schlieren images of gasoline spray were processed and the detected boundaries were overlaid on the original schlieren images. It is obvious in Fig. 7 that I_{cB} outperforms I_{cA} for the schlieren images. In Figs. 5 and 6 for shadowgraph images, both I_{cA} and I_{cB} detected the entire spray region and the only difference was found in the internal spray pattern. However in Fig. 7 for the schlieren image, some spray regions were missed out when I_{cA} was applied. One solution for this problem was to adjust the grayscale threshold until the boundary detection became successful but this resulted in a serious question of consistency in the image processing as each image required a manual selection of the thresholds. Therefore for the schlieren images in this study, we used I_{cB} to detect the boundaries of the spray droplets.

SPRAY TIP PENETRATION AND SPREADING ANGLE

The image processing and boundary detection in Figs. 5 to 7 enable measurement of the penetration and spreading angle of the spray. Figure 8 shows definitions of the spray tip penetration and spreading angle used in this study. The tip penetration was measured by calculating the distance between the nozzle and the spray droplet in the farthest downstream as shown at the figure top-left. A circle symbol is used to denote this droplet region. Note that this region can be found either in the left or right side of the image and our real-time processing software for the spray movie captured it successfully.

The spreading angle was measured using the farthest spray droplet from the nozzle: similar to the tip penetration but in the horizontal direction. In Fig. 8, a square symbol is shown to denote this region for the spreading angle measurement. It is worth to noting that the transient behavior of the spray was well observed by this method. For example, the spray at 1ms aSOI shows a much wider dispersion than that of a steady-period of injection (*i.e.* after 2 ms aSOI). Also, Fig. 8 shows that our definition of the spreading angle follows $\alpha_{80\%,}$ which is drawn as white solid lines.

Note that the same shadowgraph images of Figs. 5 and 6 are used again in Fig. 8. However, Fig. 8 shows a circular light boundary and dark regions at the corner. For the rest of the figures, the image pixels outlined as a dashed line (see the box in the image at 4ms aSOI) are presented by masking out these outer pixels. However, the tip penetration and spreading angle measurement were continued until the spray went out of the camera field of view.

The tip penetration and spreading angle of shadowgraph images are plotted in Fig. 8. To compare the effectiveness of I_{cA} and I_{cB} for the tip penetration and spreading angle measurements, the shadowgraph images of Figs. 5 and 6 were used because I_{cA} was not successful for the boundary detection for the schlieren images (see Fig. 7). One might argue the difference in the tip penetration and spreading angle between I_{cA} and I_{cB} is due to a different internal spray pattern. However, it was not a concern for the tip penetration and spreading angle because only the droplets at the spray border were used as per the definitions of this study.

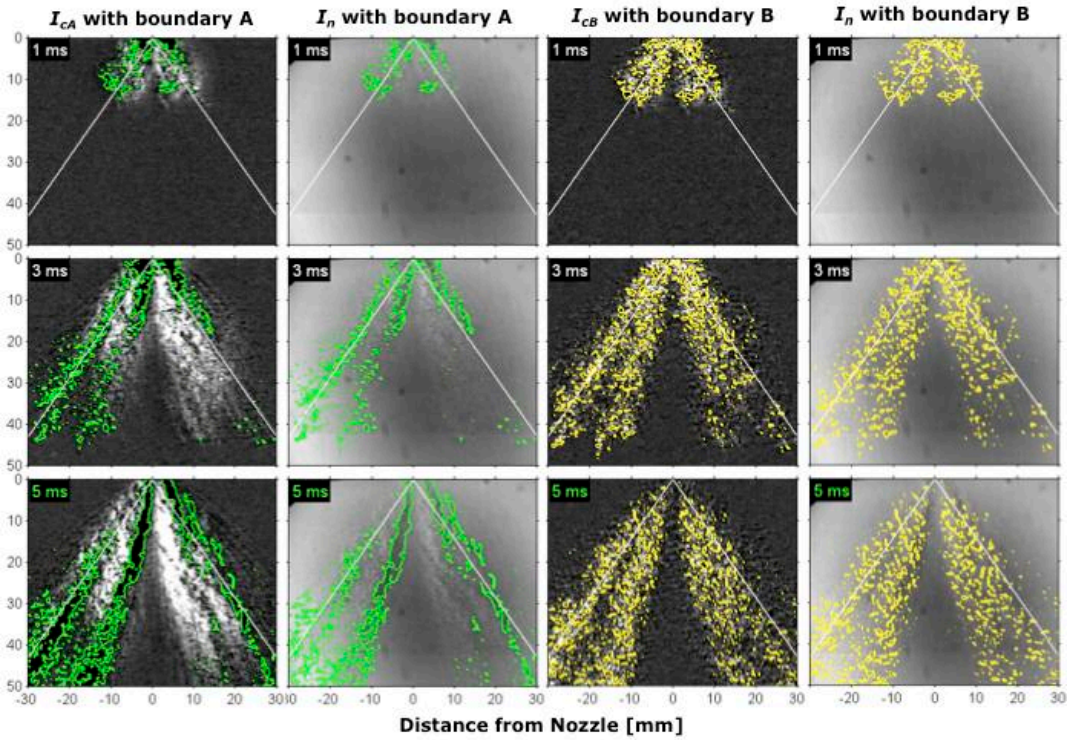

Figure 7: Spray boundaries overlaid on raw and corrected schlieren images. Both method A (left two columns) and method B (right two columns) are applied. Solid white lines are drawn using a spreading angle provided by the injector manufacturer (80% mass angle). Shown at the image top-left is time after the start of injection.

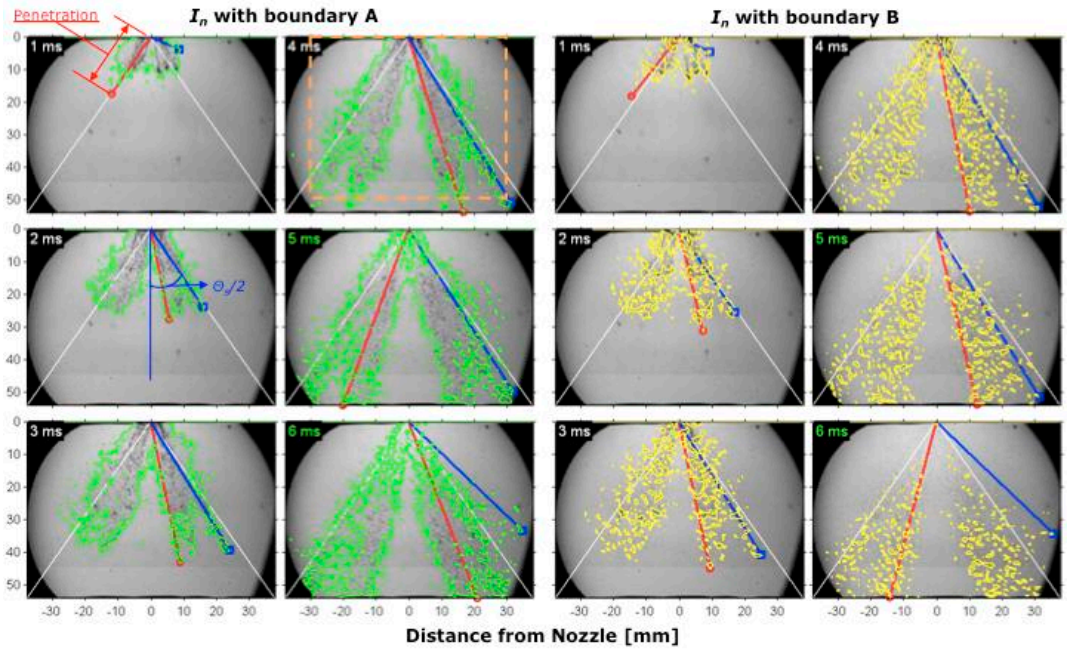

Figure 8: Image processing to determine the spray tip penetration and spreading angle. Spray images and boundaries from Figs. 5 and 6.

Figure 9 shows that the spray tip penetration increases with increasing time after the start of injection. An immediate conclusion from the figure may be drawn that the spray tip penetration and spreading angle are not sensitive to the background correction methods. The tip penetrations of I_{cA} and I_{cB} are almost identical and so is the spreading angle. Once again, this may be expected because the droplets at the spray border were used for the measurement and the difference in the spray pattern did not affect global parameters like the penetration rate and spreading angle.

There are many details to discuss in Fig. 9. For instance, sharp spikes are seen for both tip penetration and spreading angle. These are due to turbulent fluctuations of the spray since the data was from an instantaneous cycle. Also, it is interesting that in the tip penetration a discrete step change may be observed at about 1.2 ms aSOI. This is also coincident with the higher spreading angle during the initial transient. It is likely that a higher injection rate in the earlier stage of fuel injection caused a higher penetration and dispersion. Since the fuel injector has a small volume in the nozzle, fuel left in the previous injection was injected together with the fuel of the present injection, which temporarily increased the injection rate. After this initial transient, the spray tip penetration increases linearly again as shown in Fig. 9. At the same time, the spreading angle becomes nearly constant and close to $\alpha_{80\%}$.

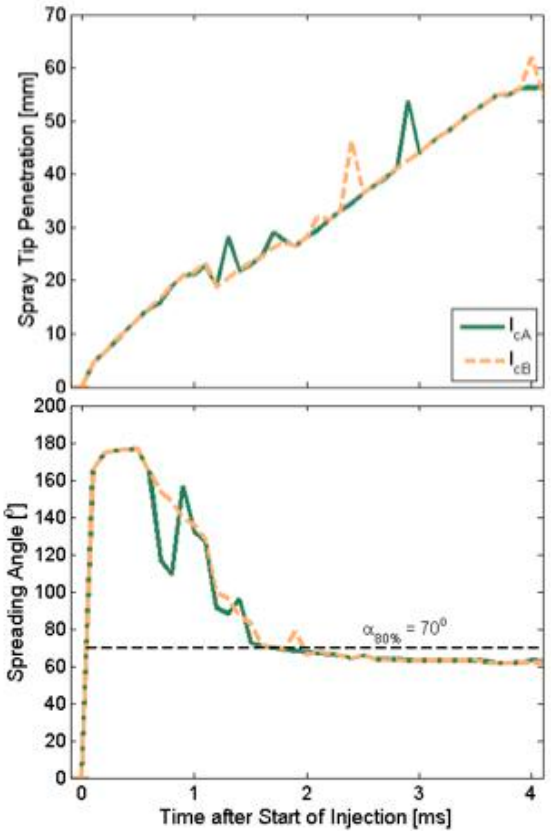

Figure 9: Spray tip penetrations determined from the spray boundaries using method A (I_{nA}) and method B (I_{nB}) in Fig. 8.

LIGHT CUT-OFF IN SCHLIEREN IMAGING

Two parameters are important in positioning the schlieren stop: the amount of light cut-off and orientation of the stop. If a higher proportion of light is blocked at the focal point, the schlieren sensitivity will increase while the overall image will be darkened. Also, if different orientations of the schlieren stop relative to the flow axis are applied, different flow patterns will be seen in schlieren images. For instance, a schlieren image taken with the knife-edge at right

angles to the flow axis will illustrate axial density gradients in the flow. Likewise, a schlieren image taken with the knife-edge parallel to the flow axis will illustrate transverse density gradients in the flow.

Figure 10 shows schlieren (background) images for various schlieren stops prior to the fuel injection. In the top row, "darkening" of the image is observed as the cut-off ratio increases. Compared to a 0 % cut-off ratio (shadowgraph), 60 % and 80 % cut-off ratios using a vertical knife-edge appear to be darker throughout the image. In the experiments, other cut-off ratios were also tested; however, 60 and 80 % proportions showed distinct differences in the spray images and

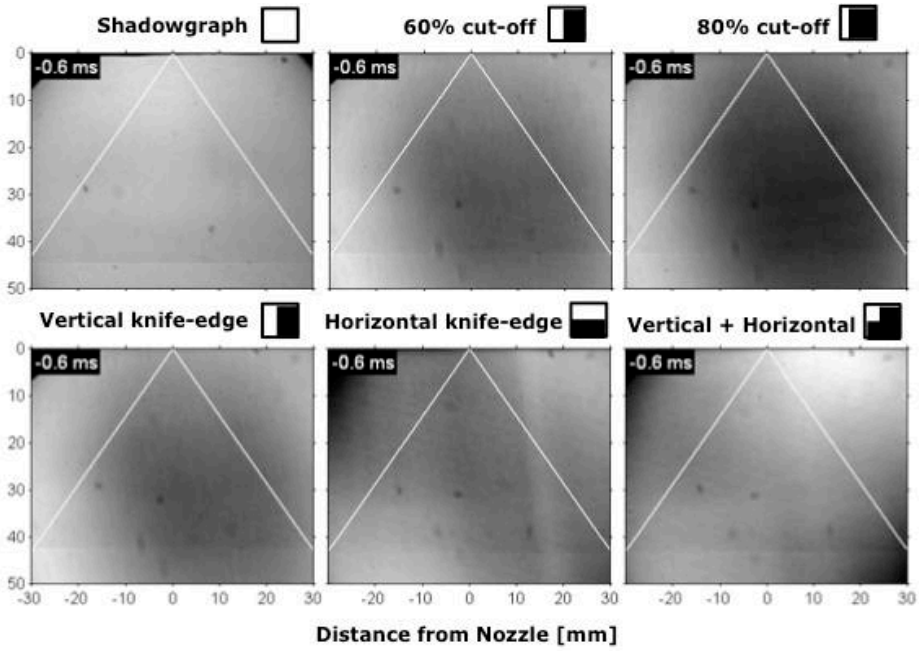

Figure 10: Schlieren images of the chamber prior to fuel injection (*i.e.* background image) for various cut-off proportions and orientations tested in this study.

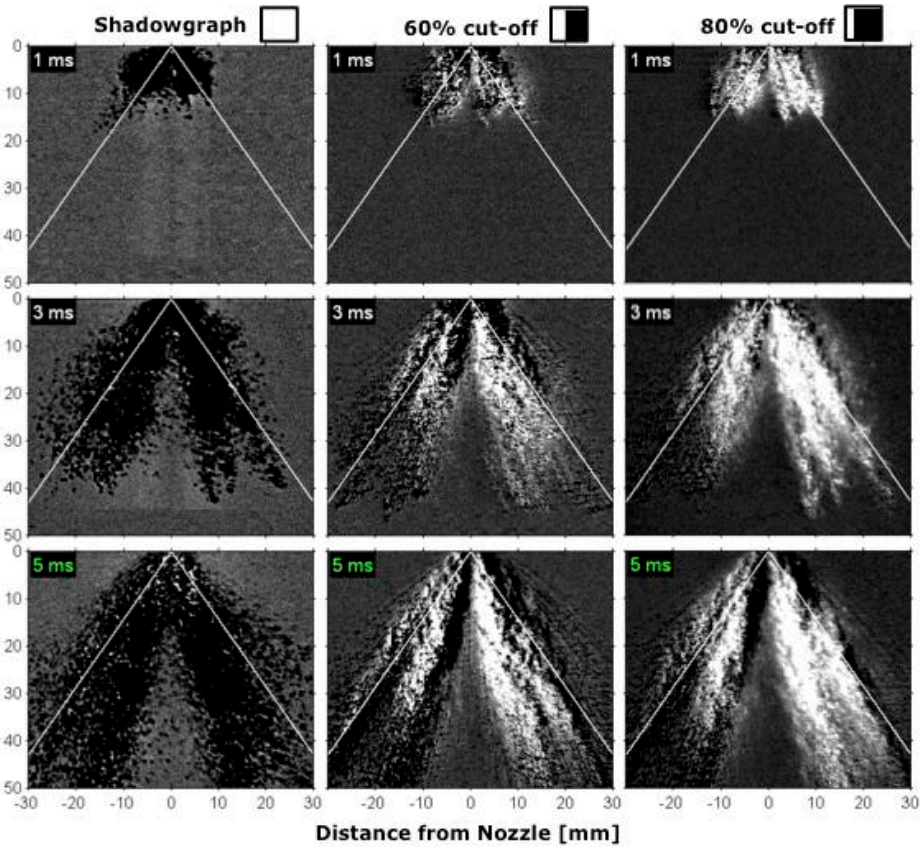

Figure 11: Effect of cut-off proportion on schlieren spray images. A vertical knife-edge is used. Solid white lines are drawn using a spreading angle provided by the injector manufacturer (80% mass angle). Shown at the image top-left is time after the start of injection.

hence were selected. In the bottom row, background images with three different schlieren stops are shown. At a fixed cut-off proportion of 60 %, we tested a vertical knife-edge and a horizontal knife-edge. A combination of these two was also examined again while 60 % cut-off ratio was maintained.

PROPORTION OF LIGHT CUT-OFF

When experimentalists setup a schlieren system, they adjust a proportion of the light cut-off until the schlieren images are optimized. The presented images in the literature, therefore, typically have the best possible quality and clarity. We followed the same approach and concluded that about 60 % cut-off performed best for the gasoline sprays of the present study. This is well demonstrated in Fig. 11. The shadowgraph images with no light cut-off show dark sprays. No internal pattern or turbulent structure can be seen in this shadowgraph. By contrast, higher cut-off ratios reveal more information in the spray pattern as shown in the second and third column of Fig. 11. Note that the schlieren images were background corrected (*i.e.* I_{cB}) and a gray-scale off-set was added, resulting in brighter spray regions than those of the shadowgraph images. At an 80 % cut-off ratio, some regions within the spray were too bright which hindered the image processing as high schlieren sensitivity was achieved at the expense of darkening in the raw images. This meant there was an optimal cut-off proportion and in this study it appeared to be 60 %.

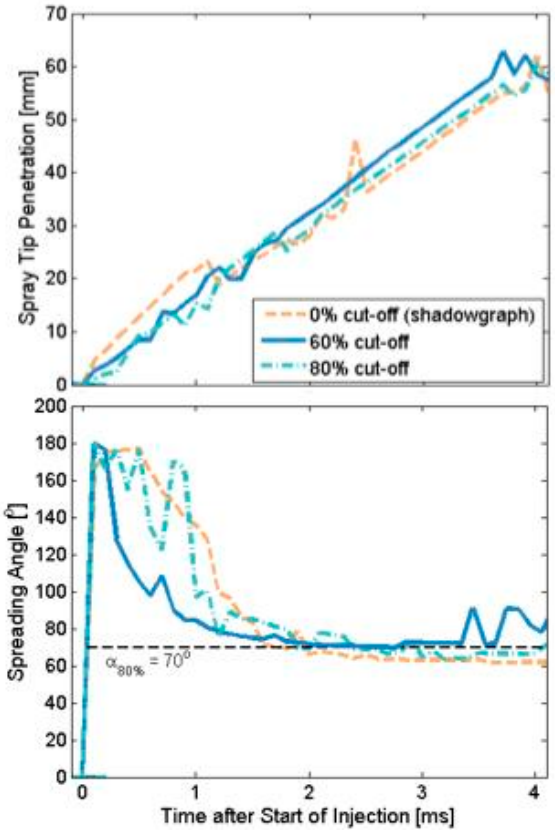

Figure 12: Effect of cut-off proportion on spray tip penetration and spreading angle determined from the spray boundaries in Fig. 11.

While issues discussed above discussion were expected, Fig. 12 shows an unexpected result. Using the image processing technique of Fig. 8, the spray tip penetration and spreading angle were determined and the results are plotted in Fig. 12. The first noticeable point from the figure is that the tip penetrations and spreading angles do not vary much for all cut-off proportions tested. If the initial transient is excluded, both the tip penetrations and spreading angles are very similar. Only difference is seen between the start of injection and about 1.5 ms aSOI. However, this initial transient is not repeatable and hence cannot be used for this discussion. In fact, no monotonic trend was found with increasing cut-off ratios either during this initial transient or for the steady period of injection. Therefore, it was concluded that high refractive-index gradients near the spray border made no difference in the tip penetration and spreading angle for varying cut-off ratios. This conclusion is consistent with Ref. [4]: essentially that the shadowgraph technique was sufficient to detect of the edge of the diesel jet. However, we do not discount the value of visual information obtained from high-sensitivity schlieren images and therefore 60 % cut-off ratio was used for the following section.

ORIENTATION OF SCHLIEREN-STOP

While how much of the light was blocked at the focal point was important for the schlieren sensitivity and in turn spray images, in what direction the knife-edge was applied was also important. For instance, if only a horizontal knife-edge is used, the schlieren imaging detects only vertical components $\partial n/\partial y$ in the schlieren object. Refractions parallel to the edge, due to $\partial n/\partial x$, move rays along it but not across it and therefore there is no change in schlieren images. A signal with purely horizontal gradients will remain invisible despite the presence of the knife-edge. This issue was addressed by varying the orientation of the knife-edges. Figure 13 shows schlieren images of the gasoline sprays for a vertical, a horizontal, and a combined knife-edge. The spray images with 60 % cut-off ratio from Fig. 11 are shown again as an example for the vertical knife-edge. Next to it, spray images with a horizontal knife-edge are shown.

From Fig. 13, one may notice that the horizontal knife-edge enhanced the schlieren sensitivity in the transverse direction. Indeed, the horizontal knife-edge shows more detail in the horizontal direction, in contrast to the vertical knife-edge that shows higher gradients in the vertical direction. As a result, the sprays appear more scattered and dispersed for the horizontal direction while more bold and stretched sprays are observed for the vertical knife-edge. Intuitively, a combination of these two should give the best result, as the spray images would be optimized in both directions. A quick answer to this question was yes, as shown in the last column of Fig. 13. The spray images with both a vertical and a horizontal knife-edge do show a better structure and pattern than the other two cases. For example, noise-like small-structures near the spray border are filtered out

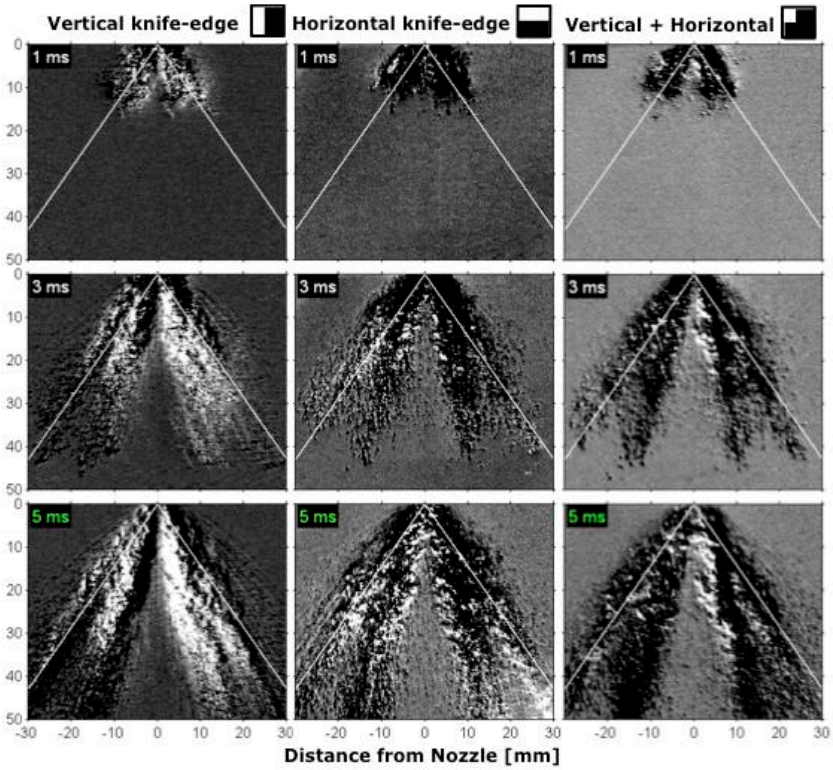

Figure 13: Effect of cut-off orientation on schlieren spray images. The cut-off proportion is fixed at 60 %. Solid white lines are drawn using a spreading angle provided by the injector manufacturer (80% mass angle). Shown at the image top-left is time after the start of injection.

and the "boldness" of the sprays is depressed resulting in both clear boundaries and turbulent structures.

While the aforementioned information from a visual inspection is important, it might be worth to measure the spray tip penetration and spreading angle for various knife-edge orientations. Figure 14 shows the results. Interestingly and similar to Fig. 12, it is clear that both the tip penetration and spreading angle are similar for all knife-edge orientations tested. The tip penetrations show an almost linear increase and spreading angles converge to $\alpha_{80\%}$ quickly after the initial transient.

There are two implications from these observations. First, the better knife-edge orientation for visualization of the spray structure and pattern appears to be that with both the vertical and horizontal cut-off. Although not quantitative, visual information from the schlieren images are valuable to study gasoline sprays. In this regard, a combination of the vertical and horizontal knife-edge provides optimized images. Second, the spray tip penetration and spreading angle are not affected by the orientations of the schlieren stop. This was because a refractive-index gradient, which was used to determine the tip penetration and spreading angle, was very strong near the spray border and therefore was not sensitive to variations of the schlieren stop.

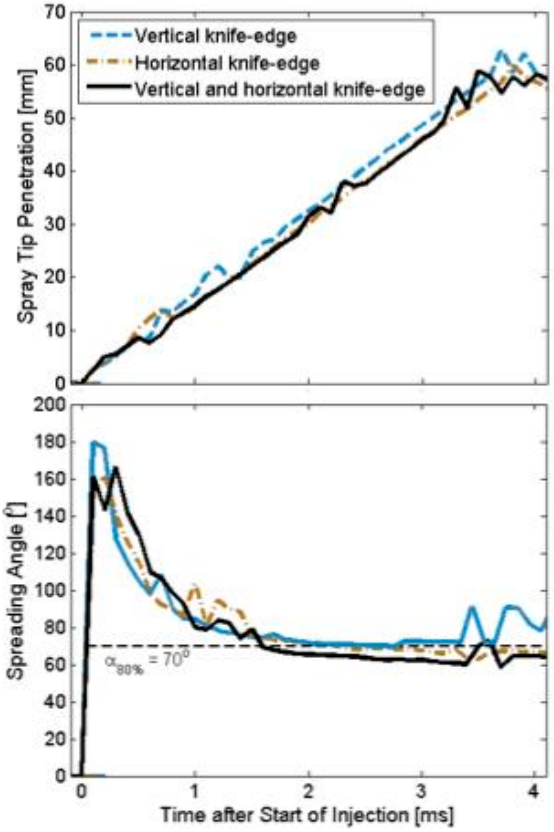

Figure 14: Effect of cut-off orientation on spray tip penetration and spread angle determined from the spray boundaries in Fig. 13.

CONCLUSION

Gasoline injection into an optical chamber simulating engine intake conditions was visualized using a high-speed schlieren system. A z-type schlieren system was used to investigate the evaporating gasoline spray structure and pattern as well as the tip penetration and spreading angle. Types of schlieren system and their principles based on the geometric theory of the refraction were summarized using a gasoline spray example. Also, details of the z-type schlieren system setup and application were shared including off-axis aberration issues, the parabolic mirror setup, the schlieren stop orientation, and the techniques used for image processing. Major findings from this study can be summarized as follows:

1. Two background correction methods were used to help detect spray boundaries: one in which the raw image was subtracted by the background obtained prior to the fuel injection and the other that used the background from a preceding image for the correction. For shadowgraph images, two methods exhibited no difference in the boundary detection. However, for schlieren images, the former method showed problem in the detection of some spray regions. Therefore, the latter correction method was used in this study.

2. The tip penetration was measured by calculating the distance between the nozzle and a spray droplet in the farthest downstream while the spreading angle was measured using the farthest spray droplet from the nozzle in the horizontal direction. The spreading angle definition used in this study matched well with the manufacturer's specification.

3. Transient behavior of sprays in the initial stage of injection was well captured in the present schlieren system. The tip penetration showed a discrete step change between this initial transient and the steady period of injection. At the same time, much higher spreading angle was measured during the initial transient. Higher fuelling rate due to fuel leftover from the previous injection was likely cause for this behavior.

4. Various schlieren stops were investigated and it was found that approximately 60% cut-off of light performed best to image the internal pattern of the gasoline sprays. Also, a vertical knife-edge enhanced the spray pattern in the vertical direction while a horizontal cut-off showed higher contrast and more turbulent spray structures in the horizontal direction. As a result, a combination of horizontal and vertical cut-offs was optimal to unveil the most of the gasoline spray pattern and structure.

5. Parameters of the schlieren stops including the cut-off ratio and knife-edge direction did not affect the tip penetration and spreading angle due to a high refractive-index gradient near the spray border.

ACKNOWLEDGMENTS

The experiments were performed at the Engine Research Laboratory of School of Mechanical and Manufacturing Engineering at the University of New South Wales. The authors would like to acknowledge that Australian Research Council supported this work via the Linkage Project (LP110100595).

REFERENCES

1. Settles, G.S., "Schlieren and Shadowgraph Techniques", Springer, 2001.
2. Naber, J. and Siebers, D., "Effects of Gas Density and Vaporization on Penetration and Dispersion of Diesel Sprays," SAE Technical Paper 960034, *SAE Transactions – Journal of Engines*, 105, 1996, doi:10.4271/960034.
3. Matsumoto, A., Moore, W., Lai, M., Zheng, Y. et al., "Spray Characterization of Ethanol Gasoline Blends and Comparison to a CFD Model for a Gasoline Direct Injector," *SAE Int. J. Engines* **3**(1):402-425, 2010, doi:10.4271/2010-01-0601.
4. Pickett, L., Kook, S., and Williams, T., "Visualization of Diesel Spray Penetration, Cool-Flame, Ignition, High-Temperature Combustion, and Soot Formation Using High-Speed Imaging," *SAE Int. J. Engines* **2**(1):439-459, 2009, doi:10.4271/2009-01-0658.
5. Fujikawa, T., Ozasa, T., and Kozuka, K., "Development of Transparent Cylinder Engines for Schlieren Observation," SAE Technical Paper 881632, 1988.
6. Ozasa, T., Kozuka, K., and Fujikawa, T., "Schlieren Observations of In-Cylinder Phenomena Concerning a Direct-Injection Gasoline Engine", SAE Technical Paper 982696, 1998.
7. Pastor, J.V., Garcia, J.M., Pastor, J.M., and Zapata, L.D., "Evaporating Diesel Spray Visualization using a Double-Pass Shadowgraph/Schlieren Imaging," SAE Technical Paper 2007-24-0026, 2007.
8. Petersen, B.R and Ghandhi, J.B., "Transient High-Pressure Hydrogen Jet Measurements", SAE Technical Paper 2006-01-0652, 2006.
9. Saanum, I., Bysveen, M., Almas, T., and Sonju, O.K., "Ignition and Combustion Characterization of Hydrogen/Methane Mixtures by Visualization in a Rapid Compression Machine (RCM)," SAE Technical Paper 2005-24-009, 2005.
10. Keller, H.E, Spring, K.R, Long, J.C and Davidson, M.W, "Comatic Aberrations", Olympus Microscopy Resource Center, http://www.olympusmicro.com/primer/java/aberrations/coma/index.html.
11. Smith, R.C., "Observational Astrophysics", Cambridge University Press, 1995.
12. Hung, D.L.S., Harrington, D.L., Gandhi, A.H., Markle, L.E., Parrish, S.E., Shakai, J.S., Sayar, H., Cummings, S.D., and Kramer, J.L., "Gasoline Fuel Injector Spray Measurement and Characterization – A New SAE J2615

Recommended Practice", SAE Technical Paper 2008-01-1068, 2008.
13. Otsu, N., "A Threshold Selection Method from Gray-Level Histograms," IEEE Transactions on Systems, Man, and Cybernetics, 9(1):62-66, 1979.
14. Kook, S. and Pickett, L.M., "Effect of Ambient Temperature and Density on Shock Wave Generation in a Diesel Engine", Atomization and Sprays 20(2):163-175, 2010.

CONTACT

Dr Sanghoon Kook: s.kook@unsw.edu.au
Lecturer of School of Mechanical Engineering
Academic-in-Charge, Engine Research Laboratory
University of New South Wales

ISSN 0148-7191

SAE Customer Service:
Tel: 877-606-7323 (inside USA and Canada)
Tel: 724-776-4970 (outside USA)
Fax: 724-776-0790
Email: CustomerService@sae.org
SAE Web Address: http://www.sae.org
Printed in USA